Magnetization and antiferromagnetic coupling of the interface between a 20 nm $Y_3Fe_5O_{12}$ film and $Gd_3Ga_5O_{12}$ substrate

M. J. Roos,[1] P. Quarterman,[2] Jinjun Ding,[3] Mingzhong Wu,[3] B. J. Kirby,[2] and B. L. Zink[1,*]
[1]*Department of Physics and Astronomy, University of Denver, Denver, Colorado 80208, USA*
[2]*NIST Center for Neutron Research, National Institute of Standards and Technology, Gaithersburg, Maryland 20899, USA*
[3]*Department of Physics, Colorado State University, Fort Collins, Colorado 80523, USA*

(Received 22 September 2021; accepted 24 February 2022; published 9 March 2022)

We present evidence for and characterization of a ≈4-nm-thick $(Y_{1-x}Gd_x)_3Fe_5O_{12}$ layer with $x \geqslant 0.4$ formed at the interface between a gadolinium gallium garnet (GGG) substrate and a sputtered $Y_3Fe_5O_{12}$ (YIG) epitaxial film with nominal thickness of 20 nm. Temperature-dependent polarized neutron reflectometry (PNR) and superconducting quantum interference device (SQUID) magnetometry show antiferromagnetic alignment of this interfacial layer with the bulk of the YIG film at low T that persists to at least 3 tesla. These experiments also show that this interfacial alignment switches from antiparallel to parallel between 100 and 200 K in small applied magnetic fields. Simple modeling suggests correlation of this crossover with the ferrimagnetic compensation point of the mixed garnet that forms this interfacial layer.

DOI: 10.1103/PhysRevMaterials.6.034401

I. INTRODUCTION

Yttrium iron garnet $Y_3Fe_5O_{12}$ (YIG) is a wide band-gap (2.8 eV) ferrimagnet with exceptionally low Gilbert damping with important technological applications in RF and microwave engineering [1,2]. In recent years YIG has become nearly ubiquitous in spintronics, where it is commonly used as a spin source (via spin pumping [3–8] and/or the longitudinal spin Seebeck effects [9–12]), or as a magnon spin current channel [13–19]. Though some applications and investigations use bulk YIG in very high-quality single crystals, many focus on films of various thickness grown by liquid phase epitaxy, pulsed laser deposition, or sputtering [20]. These include microwave delay lines, auto-oscillators, and magnonic crystals [21–25]. The best available substrate for YIG thin film growth in terms of lattice match is gadolinium gallium garnet $Gd_3Ga_5O_{12}$ (GGG), and this is by far the most common substrate for YIG thin films over a wide range of thickness.

As all forms of this thin film growth typically rely on reaching temperatures near 700 °C either during growth or in a postgrowth annealing step, and considering the similar chemical properties of Y and Gd, interdiffusion at the YIG/GGG interface is not surprising. This is one explanation put forward for recent observations of an interfacial layer and/or antiferromagnetic coupling that forms between the YIG and the GGG [26–34]. Modification of magnetic properties at an interface is, of course, common for a variety of reasons [35]. Some form of modified magnetic order, with an awareness of the likely role of interdiffusion of atomic species at the film/substrate interface has been discussed for YIG for some decades. LeCraw *et al.* [36] argued, based on magnetic domain imaging, that garnet films grown by liquid phase epitaxy (LPE) and annealed at 1100 °C experienced diffusion of Ga.

More recent reports using more powerful experimental probes have refined this view. Studies using the magneto-optical Kerr effect (MOKE) and spectral ellipsometry on 6−30-nm-thick YIG films sputtered at ambient temperatures onto GGG substrates and postannealed at 800 °C provided evidence for a layer at the YIG/GGG interface with magnetization aligned antiparallel to that of the YIG [26]. Further evidence of modified magnetism at the YIG/GGG interface came from polarized neutron reflectometry (PNR) [29], though that study argued for a nonmagnetic interfacial layer. Suturin *et al.* also reported a magnetically "dead" interfacial layer based on PNR, x-ray reflectometry and spectroscopy, and secondary ion mass spectrometry on YIG/GGG grown via laser molecular beam epitaxy at 700° growth temperature [31]. This group also suggests Ga interdiffusion is responsible. Gomez-Perez *et al.* used spin Hall magnetoresistance and x-ray circular dichroism to again argue for an antiferromagnetically-coupled interface layer in a 13-nm film grown on a GGG substrate via pulsed laser deposition [30].

Scanning tunneling electron microscopy with energy dispersive x-ray spectroscopy reported in that paper argued that the interface layer is formed from gadolinium iron garnet (GdIG), where Gd entirely replaces Y in the synthetic garnet structure. This replacement can occur with little energy cost since Y and Gd are chemically similar, though the addition of the Gd 4f shell magnetic moment causes large magnetization at low temperature and the interaction between the Gd and Fe moments introduces a lower ferrimagnetic compensation temperature. In bulk, mixed rare-earth garnets, $(Y_{1-x}Gd_x)_3Fe_5O_{12}$, have been shown to have a composition-dependent ferrimagnetic compensation temperature, which reduces from near 300 K for pure GdIG to <50 K for $x = 0.1$ [37]. All compositions maintain the much higher temperature

*Corresponding author: barry.zink@du.edu

(near 550 K) magnetic transition seen in pure YIG. Ferromagnetic resonance (FMR) studies also indicate modified or antiferromagnetically coupled interfacial layers in various YIG thin films on GGG [33,38]. Though most of these reports detail a modified magnetic structure in these heteroepitaxial YIG/GGG samples, this interface is not completely understood. This is partly due to the challenge presented for traditional magnetometry by the very large paramagnetic background from the GGG substrate.

GGG, though commonly considered to be a simple paramagnet, is a frustrated Heisenberg magnet with a Curie-Weiss temperature near -2 K. However, the frustration prevents observable magnetic ordering until much lower temperatures [39]. At higher temperatures the gadolinium moments give GGG a large paramagnetic susceptibility. The large paramagnetism presents obvious challenges for magnetometry of nm-scale thin films grown on GGG substrates [27,28,40,41]. For this reason, quantitative magnetometry of YIG films on GGG substrates is rare, especially exploration of the temperature (T) dependence at low T where the GGG background magnetization grows very large. Mitra *et al.* did present SQUID magnetometry of YIG films with thickness 40 nm and greater grown on GGG substrates via RF reactive sputtering [28]. These show reduced magnetization from bulk YIG values at all temperatures, though the model the authors present considers an antiferromagnetically coupled layer at the YIG-GGG interface that contributes only below 100 K. At low temperatures, a reduction in moment was seen that grew largest for the thinnest reported sample, and with support of PNR and electron microscopy, Mitra *et al.* suggested an interdiffusion of Y and Gd in a 4−6-nm-thick layer at the interface.

In this paper we present results of polarized neutron reflectometry (PNR) and SQUID magnetometry vs T, with careful consideration of the background GGG substrate subtraction, on a nominally 20-nm-thick sputtered YIG thin film. PNR confirms not only the presence of an antiferromagnetically coupled $(Gd_xY_{1-x})_3Fe_5O_{12}$, or (Gd-Y)IG, layer, but also that this layer retains its moment and antiferromagnetic alignment to the YIG at low T even in very large applied field. PNR also shows a crossover from antiferromagnetic to ferromagnetic alignment of the interfacial and YIG films between 100 K and 200 K. To perform SQUID magnetometry we subtract the background contributions determined by performing exactly the same field sweeps on a companion GGG substrate with no YIG, to isolate the magnetic contribution of the interface layer and YIG film. These measurements again confirm the presence of a magnetic (Gd-Y)IG interface layer, that shows antiferromagnetic alignment with respect to the YIG at low T, with a crossover near that seen in PNR. Estimated modeling of the magnetization argues that the ∼3.6-nm-thick interfacial layer has a fairly high concentration of Gd, and suggests that the change in interfacial coupling could be tied to the ferrimagnetic compensation point of the mixed garnet interfacial layer.

II. EXPERIMENT

We grew a nominally 20-nm-thick YIG layer on a GGG substrate via RF sputtering at ambient temperature. After sputtering, the film was annealed at 800 °C in 1.1 Torr (147 Pa) partial O_2 pressure for 240 min. Further details of the growth technique and typical resulting damping parameter and other properties are discussed elsewhere [40,42]. The GGG was purchased commercially [43] as a 0.5-mm-thick, 10 mm by 10 mm square, and cleaved to ≈5 mm × 5 mm for use as substrates.

Model fitting of specular PNR data allows us to infer the depth profiles of the complex nuclear scattering length density ρ_N indicative of the nuclear composition, and the magnetic scattering length density ρ_M, which is proportional to the in-plane magnetization M for thin films and multilayers [44]. We conducted PNR measurements using the polarized beam reflectometer at the NIST Center for Neutron Research. An incident 0.475-nm neutron beam was polarized with magnetic moment parallel (+) or antiparallel (–) to a magnetic field H applied along the plane of the sample. We measured the spin analyzed nonspin-flip specular reflectivities $--$ and $++$ as functions of wave vector transfer Q along the sample growth axis. We collected data both as a function of varying T and H as described below.

We reduced the PNR data using Reductus [45], and performed model fitting using Refl1D [46]. We simultaneously fit data for all T and H conditions to a single universal model with a fixed nuclear profile and condition-dependent magnetic profiles. As described in more detail below, the data could not be represented with a simple model corresponding to a single YIG layer on a GGG substrate. The data are well fit with a model featuring a magnetically distinct sublayer at the YIG/GGG interface, similar to previous reports [28,29,31,47]. We calculated the GGG and noninterfacial YIG layer ρ_N values using bulk density values and the wavelength-dependent scattering lengths of the constituent isotopes [48,49], which we treated as fixed parameters. We note that Gd is the only element in the sample with an appreciable imaginary ρ_N component. The magnetically distinct region at the GGG/YIG interface is likely a result of diffusion of chemical species. For our model, we approximate this phenomenon using a single layer with fitted and rough interfaces [50]. As GGG is essentially paramagnetic at the temperatures measured, the magnetization of the GGG substrate was constrained to be parallel to the applied field direction (i.e., $\rho_N > 0$). This constraint is consistent with SQUID measurements, and lifting it does not appreciably affect the fit quality. We determined fitting parameter uncertainties using a Markov chain Monte Carlo algorithm [51] packaged with Refl1D. The average two standard deviation uncertainty for PNR-determined magnetization values is approximately 5 kA/m. It is important to note that these uncertainties are based on known statistical uncertainty in the data, and do not account for potential systematic error in the measurements, or uncertainty associated with choice of model. All uncertainties given for fitting parameters correspond to two standard deviations, while uncertainties shown for scattering data correspond to one standard deviation.

We performed SQUID magnetometry in a commercial system equipped with integral magnetic shielding, with magnet reset capabilities and a 7-T magnet, with automated temperature control from 2 K to 400 K using a reciprocating sample method to increase the signal-to-noise ratio [52].

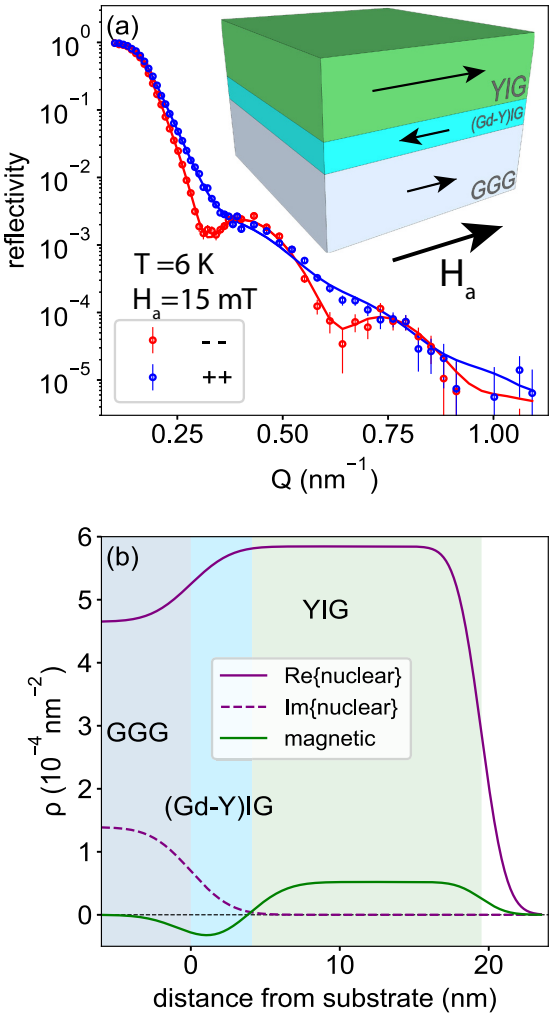

FIG. 1. (a) Polarized neutron reflectivity data measured at 6 K and 15 mT for both spin analyzed nonspin-flip specular reflectivities, $++$ (blue symbols), and $--$ (red symbols), with fits shown as solid lines. Inset: Schematic view of the sample showing GGG substrate, (Gd-Y)IG interfacial region, and YIG film, with magnetization corresponding to conditions of this measurement shown schematically with black arrows. (b) Nuclear ρ_N, and magnetic ρ_M, scattering length-density profiles determined from fits to the data.

The YIG/GGG sample and the companion substrate were nearly equal size, and mounted in the magnetometer using the same techniques. Samples were mounted in a laminar flow hood using dedicated nonmetallic tools and clean gloves to minimize contamination from dust and other potential sources of magnetic contamination. We took care to replicate both temperature and magnetic histories by using identical measurement sequences on substrate and sample, and the magnet was reset before each measurement to minimize trapped flux.

III. RESULTS AND DISCUSSION

Figure 1(a) shows example polarized neutron reflectivity data for the YIG/GGG sample at 6 K measured in an applied field of $\mu_o H = 15\,\text{mT}$ ($H = 150$ Oe). This field is much larger than the expected coercive field H_c of YIG. We plot reflectivity vs neutron wave vector Q for both neutron spin polarizations. The fitted data features clear, well-represented, spin-dependent oscillations. Figure 1(b) shows the corresponding nuclear (ρ_N) and magnetic (ρ_M) scattering length density vs distance perpendicular to the substrate z, where an additional (Gd-Y)IG layer between the GGG substrate and bulk-like YIG was necessary to adequately model the data. These three regions: the GGG substrate, the ≈4-nm (Gd-Y)IG, and the 15.9-nm YIG film, are indicated by background shading. Testing of different models showed that our sensitivity to the nuclear profile is insufficient to reliably characterize the chemical composition of the nominal (Gd-Y)IG layer. We can tell that the interfaces are rough, but cannot uniquely distinguish if the interfacial layer results from an off stochiometric Gd composition or Ga diffusion, both of which have been reported in the literature [28,31,36]. While ρ_M is small compared to ρ_N, it gives rise to distinct spin-dependent features in the data that yield high confidence in ρ_M for the individual layers. Thus, we can conclude that at low T near the YIG remanence, the GGG is only weakly magnetized, while the YIG and (Gd-Y)IG layer magnetizations are oriented antiparallel to one another, with the YIG magnetization tracking the direction of H.

The depth sensitivity demonstrated in Fig. 1 allows for layer resolved magnetometry, as shown in Fig. 2 with T dependencies in 15 mT (left column) and 3 T (right column). The T-dependent fitted data are shown in panels (a) and (b) as spin asymmetry (difference in $++$ and $--$ divided by their sum), which is a useful quantity for visualizing changes in the magnetic scattering when the nuclear contribution to the scattering can be assumed to be static. The magnetic profiles are shown in panels (c) and (d), plotted in units of magnetization (1 kA/m = 1 emu/cc) vs z. Panels (e) and (f) summarize the profiles in a more familiar plot of $M(T)$ for each layer. The two sigma statistical uncertainties for these fitting parameter values are too small to be seen at this scale.

At 15 mT, a modest field but well above expected in-plane coercive field H_c for the YIG film, the YIG magnetization tracks very closely to the expected $M(T)$ for bulk YIG, shown as a dotted red line [37]. The interfacial (Gd-Y)IG layer magnetization stays antiparallel to H up to 150 K, where it crosses over to become weakly positively magnetized, suggesting that the interlayer antiferromagnetic coupling between the two layers weakens considerably over this temperature range. The 3 T $M(T)$ in Fig. 2(f) shows little change for the YIG magnetization, as expected given the material's low coercivity. The GGG $M(T)$ also behaves as expected, showing a roughly $1/T$ dependence, dominated by a very large low-T magnetization induced by the very large field. This largely paramagnetic response at low T approaches zero above 50 K. Remarkably, the magnetization of the (Gd-Y)IG layer is negative at low T, and only approaches zero kA m^{-1} above 100 K. Note that the large paramagnetic contribution from the GGG at $T = 7$ K makes the very substantial negative peak from the interface layer somewhat less visually obvious. The fitting of the three components clearly identifies large negative contributions from the interface at low T. Thus, we see that even a 3-T applied field is insufficient to fully reverse the magnetization of the interfacial layer, demonstrating the strength of the antiferromagnetic interlayer exchange.

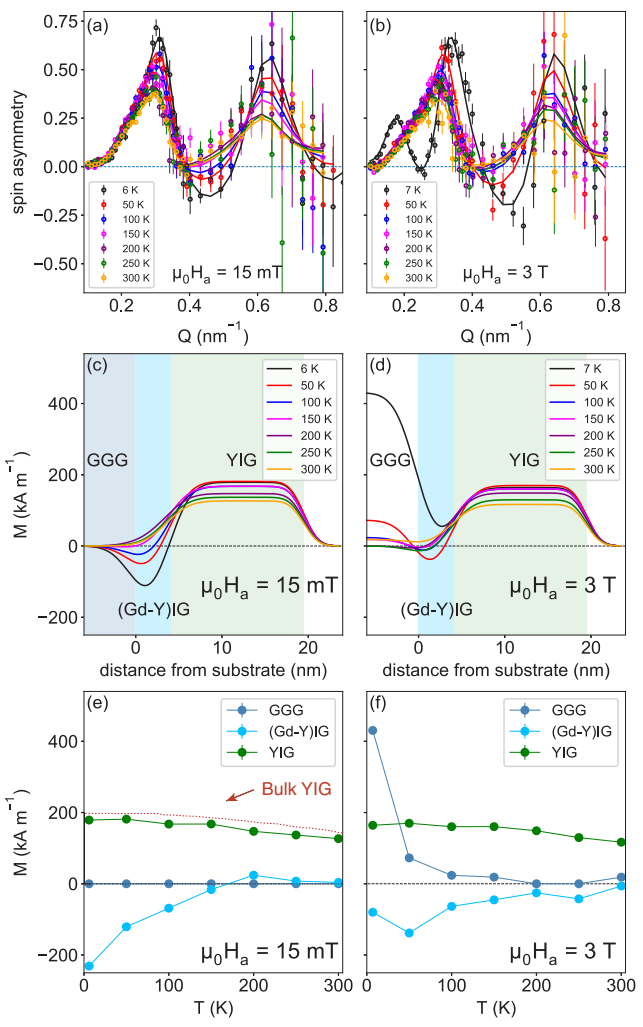

FIG. 2. PNR spin asymmetry [(a), (b)], magnetization profiles determined from model fitting [(c), (d)], and resulting M vs T measured for $\mu_0 H = 15$ mT (left) and $\mu_0 H = 3$ T (right). The three magnetic components of the sample are shown in background shading in panels (c) and (d), and their M separately plotted in (e) and (f). We provide bulk values of $M(T)$ for YIG for comparison in panel (e).

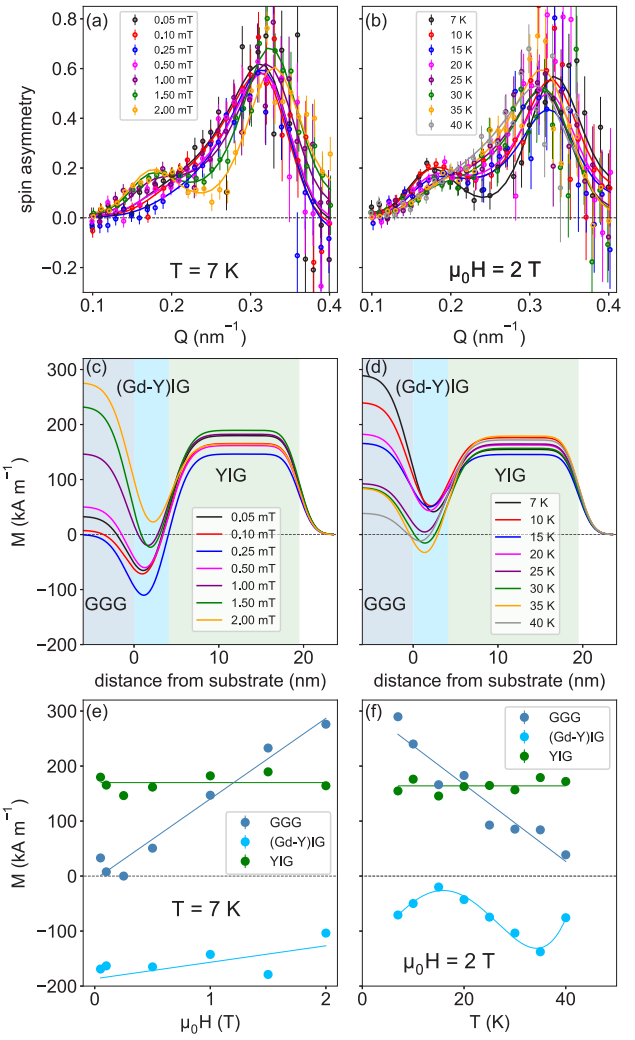

FIG. 3. PNR spin asymmetry [(a),(b)], modeled magnetization profiles [(c),(d)], and resulting M vs $\mu_0 H$ at fixed $T = 7$ K (e) and M vs T at fixed $\mu_0 H = 2$ T (f). Solid lines in (e) and (f) are guides to the eye. Possible nonmonotonic behavior of the (Gd-Y)IG layer could result from frustrated domains in this interfacial layer. Note however that the negative M at all $\mu_0 H$ for the (Gd-Y)IG indicates very strong antiferromagnetic exchange at the interface.

Figure 3 shows layer resolved $M(H)$ at 7 K (left column) and a small T-step $M(T)$ at 2 T. As in Fig. 2, panels (a) and (b) show spin asymmetry, panels (c) and (d) show the magnetization depth profiles determined from model fitting of the data, and panels (e) and (f) show the associated layer-resolved $M(H)$ and $M(T)$, respectively. Solid lines in (e) and (f) are guides to the eye. As expected for a ferromagnet well below T_c, the YIG magnetization is essentially constant with both field and temperature. The GGG also behaves intuitively, with linear field and temperature responses characteristic of a paramagnet. The (Gd-Y) magnetization shows a linear increase with H, as the Zeeman energy begins to overcome the antiferromagnetic interlayer exchange. The temperature dependence of the (Gd-Y)IG layer magnetization is more complex, deviating considerably from a monotonic response. This is suggestive of a frustrated domain state in the interfacial layer at low T. However, while the deviation is outside our statistical uncertainty (approximately 5 kA/m, error bars too small to be seen on this scale), we cannot rule out the possibility that this is an artifact associated with unaccounted uncertainty in the modeling. To wit, the YIG and GGG magnetizations in (e) and (f) also show much less pronounced but still statistically significant—and likely unphysical—degrees of nonmonotonicity.

We note that the magnetization values shown in Figs. 2(e) and 2(f) and Figs. 3(e) and 3(f) differ slightly from the corresponding profile values shown in Figs. 2(c) and 2(d) and Figs. 3(c) and 3(d). This is because the profiles show weighted averages of the (Gd-Y)IG layer with that of the neighboring GGG and YIG layers, while the $M(T)$ and $M(H)$ plots show parameter values corresponding to the inherent magnetization of the (Gd-Y)IG layer [53]. However, we emphasize that the qualitative conclusions drawn in this paper are the same regardless of which values are considered.

Quantitative measurement and analysis of the magnetization of the same sample via SQUID magnetometry requires careful consideration of the large substrate background. Figure 4(a) plots $\chi = M/H$ vs T from 2 K to 300 K measured in a single experimental run at fixed $\mu_0 H = 10$ mT (100 Oe). As expected for a paramagnet, $\chi \propto 1/T$. The red line is a fit to the Curie-Weiss law, $\chi = A/(T - \theta)$, with $\theta = -2.1$ K, which is in line with expectations for GGG. Figures 4(b) and 4(c) compare the total moment m of the YIG/GGG and companion bare GGG substrates measured over a small H range at 300 K and 10 K, respectively. At 300 K, the GGG background is small enough to clearly resolve the YIG ferromagnetic contribution on this scale, while at 10 K, the background paramagnetic contribution is already large compared to the more weakly T-dependent YIG ferromagnetism. The slight difference in the total moment for the sample and background that is obvious at 10 K is caused by a small size difference between the two substrates, which we scale appropriately in the following comparisons. In these small H scans, the GGG appears mostly as a simple paramagnet. As we describe in more detail elsewhere [54], larger field M vs H scans on GGG can cause measurement artifacts driven by trapped flux in the superconducting magnet used in the magnetometer. Here we avoid these artifacts by using this small field range and subtracting the GGG background measured under the same field and temperature sequences.

Figure 5 shows M vs $\mu_0 H$ for the YIG/(Gd-Y)IG/GGG sample, where we have subtracted the background M measured on the companion GGG substrate using the same ±5 mT field scan sequences for both, after scaling by the measured mass ratio of the two substrates to correct for the small volume mismatch. As seen in Fig. 5(a), at 300 K this leaves the low-coercivity ferromagnetic behavior of the YIG, with a symmetric saturation and slight shift on the $\mu_0 H$ axis that cannot be clearly separated from trapped flux in the magnet. As T drops, the loops all show the expected ferromagnetic hysteresis pattern, with clearly defined saturation, though with monotonically increasing coercive field. Some loops, most clearly the 10 K loop in panel (h) that shifts almost entirely above $M = 0$, show an apparent vertical shift, though this shift is not monotonic with T. Similar vertically shifted loops have been attributed to pinned moments in magnetic heterostructures involving antiferromagnetic exchange coupling [55–57]. However, considering the possible artifacts introduced by the large GGG paramagnetism interacting with trapped flux [54], we cannot attribute these shifts to the antiferromagnetic exchange coupling between the YIG and (Gd-Y)IG layers.

In Fig. 6(a) we report saturation magnetization, M_s vs T, determined from M vs H loops as shown in Fig. 5. To isolate the contribution of the thin film, we calculate M_s via:

$$M_s = \frac{M_{+,\mathrm{avg}} - M_{-,\mathrm{avg}}}{2}, \tag{1}$$

where $M_{+,\mathrm{avg}}$ and $M_{-,\mathrm{avg}}$ are averaged values of saturated M on the positive and negative field branches of the loops, respectively. This cancels the vertical shift apparent in some

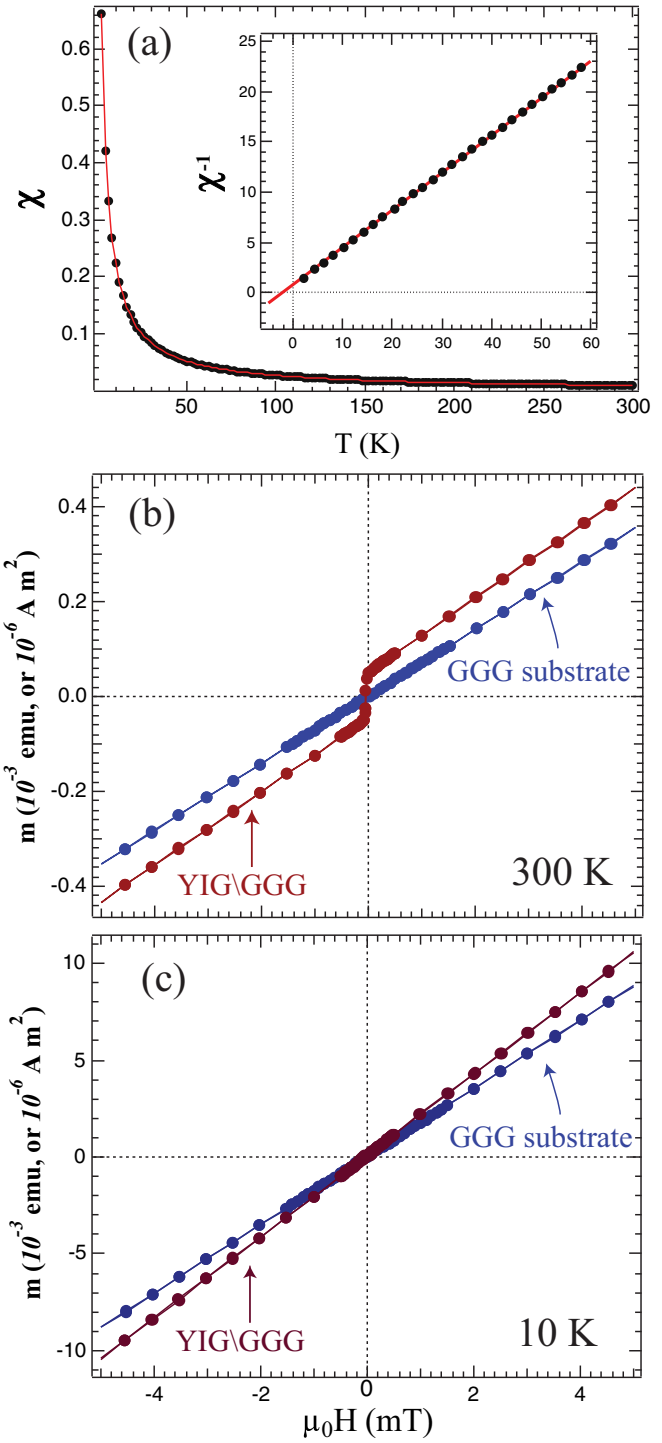

FIG. 4. (a) $\chi = M/H$ vs T for the bare GGG substrate in $\mu_0 H = 10$ mT vs T from 2 K to 300 K. Inset: $1/\chi$ vs T. In both the red line is a fit to the Curie-Weiss law with a small negative θ, as expected for GGG. (b) m vs $\mu_0 H$ at 300 K for the GGG substrate and the YIG/(Gd-Y)IG/GGG sample. At this T both the large paramagnetic contribution from the GGG and the essentially ferromagnetic contribution from the YIG are obvious even without background subtraction. (c) m vs $\mu_0 H$ at 10 K, where the paramagnetic background dominates the ferromagnetic signal. The different slopes are due to a slight difference in the substrate volume.

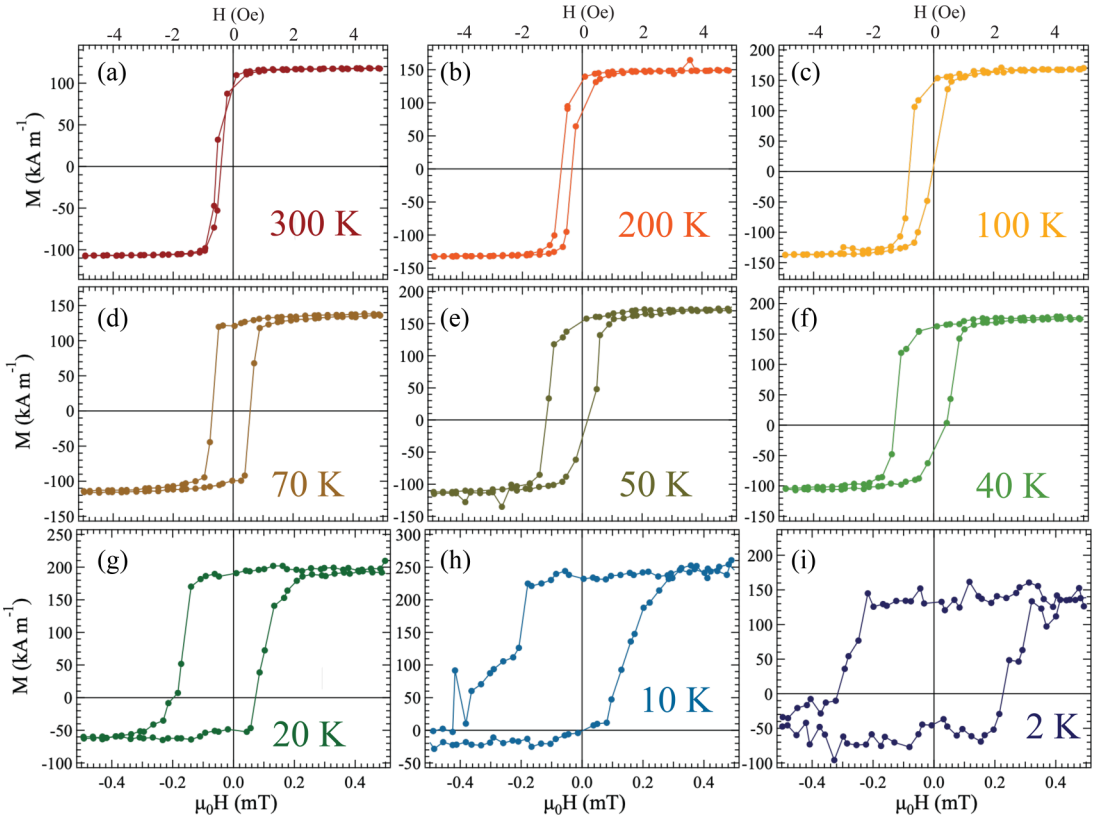

FIG. 5. M vs $\mu_0 H$ loops for the YIG/(Gd-Y)IG/GGG sample after subtraction of the matched GGG background for a series of temperatures: (a) 300 K, (b) 200 K, (c) 100 K, (d) 70 K, (e) 50 K, (f) 40 K, (g) 20 K, (h) 10 K, and (i) 2 K. All loops show the expected FM hysteresis and positive remanence, with H_c growing as T drops. Neither the small shift on the $\mu_0 H$ axis nor the shift on the M axis can be clearly linked to the YIG/(Gd-Y)IG, as discussed in the main text.

loops. In Fig. 6(a), the blue symbols indicate this M_s, which is calculated using the entire volume of the deposited film, with its total nominal thickness of 20 nm. Data was taken in two separate runs in the magnetometer, indicated by circles and squares. These show slight deviations, though not outside the estimated error bars. We compare this to the M_s calculated using a very typical procedure for substrate background subtraction where a linear background is fit to the highest H data and subtracted. This is shown using grey data points, which underreports M_s compared to the more accurate procedure, which uses carefully matched measurements of a companion GGG substrate. We also compare to M_s vs T reported for bulk YIG (red line) [37]. The measured values fall below the bulk YIG expected values at all T, which is due at least in part to the interfacial layer with its antiferromagnetically aligned low T moment.

We report H_c vs T determined from the same loops in the inset to Fig. 6(a). H_c rises as T drops roughly following $1/T$, growing largest in the T regime where M_s drops sharply. An increase in H_c of this type can be driven by thermal fluctuations and also enhanced by exchange coupling with an antiferromagnetic layer [58–62]. Typically this AF/FM coupling also introduces exchange bias. Here we cannot identify a systematic shift of the loops, potentially again due to issues related to trapped flux. However, the lack of a well-defined exchange bias could indicate that the coercivity increase is dominated by decreasing thermally-driven depinning of domain walls rather than interfacial effects.

In Fig. 6 we explore a simple model of the YIG/(Gd-Y)IG/GGG system. The blue data points plot total measured moment, m vs T, and we compare this first to bulk YIG M_s values multiplied by the volume resulting from a 15.9-nm-film thickness as determined by PNR (Figs. 1 and 2), indicated by the dashed red line. At the lowest T the total m falls far below the values for bulk YIG, where the interfacial moment is large and antiferromagnetically aligned with the YIG. As T grows, m approaches the bulk YIG values. As seen more clearly below, above $\sim 100 - 200$ K the measured moment rises slightly above the bulk YIG moment, which is in line with PNR measurements that indicate a crossover from AF to FM alignment of the interfacial layer with the YIG near this temperature at these modest applied H. We provide upper and lower estimates of the contribution of the 3.6 nm interface layer again by simple scaling of published bulk $(Gd_xY_{1-x})_3Fe_5O_{12}$ values [37]. The dark-yellow and green curves show the expected moment of 3.6-nm-thick layers with $x = 1$ (pure GdIG) and $x = 0.6$, respectively. We show the resulting estimates of the total magnetization from subtracting the interface magnetization from the 15.9-nm bulk-like YIG layer in brown and dark-green dashed lines. Though this modeling is only qualitative, we can argue that the interfacial layer is more likely to have a high concentration of Gd, since

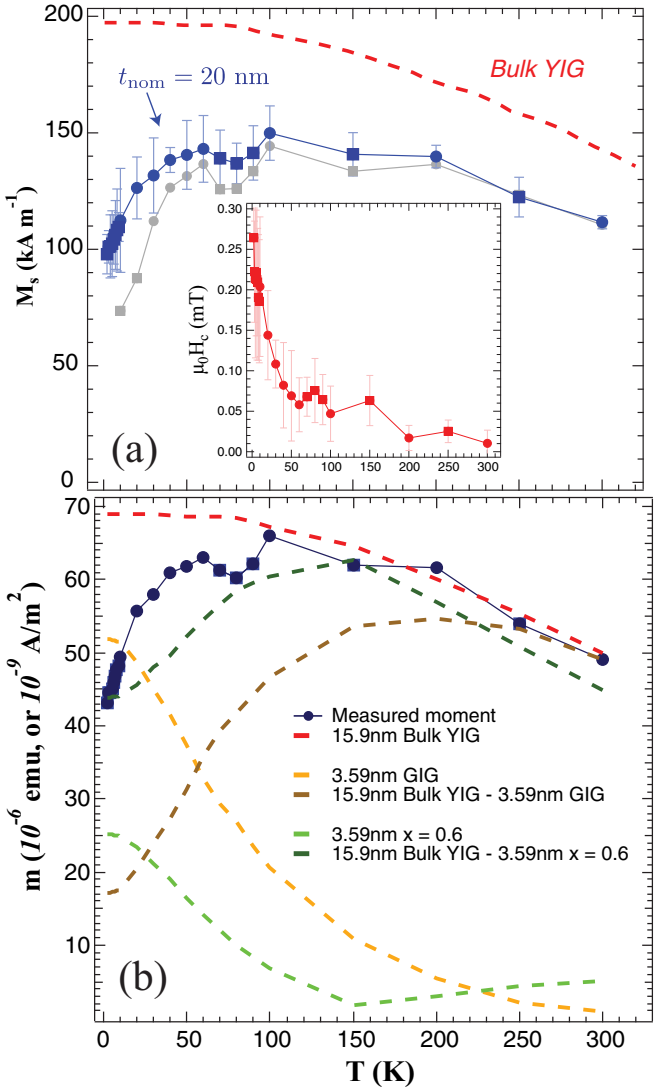

FIG. 6. (a) M_s vs T for the YIG/(Gd-Y)IG films. The blue data points show M_s with volume calculated for the entire nominal film thickness t_{nom} = 20 nm. M_s falls below bulk YIG values (dashed-red line) at all T. The grey data points show M_s when a simple linear background is assumed, instead of using the measured GGG values. Inset: $\mu_0 H_c$ vs T shows a monotonically decreasing trend. (b) Measured moment m of the YIG/(Gd-Y)IG layer (blue) compared to calculated values for a 15.9-nm-thick layer of bulk YIG (dashed-red line), 3.6-nm-thick layers of $(Gd_xY_{1-x})_3Fe_5O_{12}$ with $x = 1$ (GdIG, dark-yellow line), and $x = 0.6$ (green line), and two models subtracting these two contributions to reflect the antiferromagnetic alignment (brown and darker green lines).

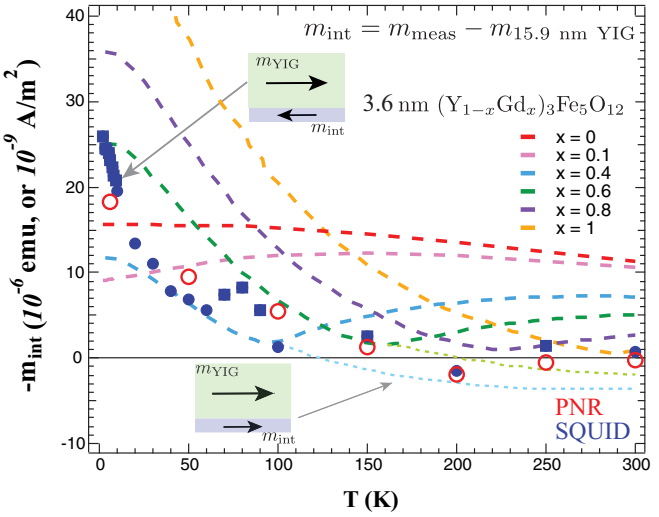

FIG. 7. Estimated moment of the (Gd-Y)IG interface layer, $-m_{int}$ vs T from SQUID magnetometry (blue symbols), and PNR (red circle) compared to bulk values of $(Gd_xY_{1-x})_3Fe_5O_{12}$ for various x (dashed lines). For the $x = 0.4$ and $x = 0.6$ mixed garnets we also show the moment with reversed sign above T_{comp}, which roughly brackets the measured $-m_{int}$ from both PNR and SQUID at high T. At low T, $-m_{int}$ again falls roughly between the values for $x = 0.4$ and $x = 0.6$, suggesting that the interface layer has a high Gd content, though is most likely not purely bulk-like GdIG.

at low T the total moment falls near the modeled values for $x = 0.6$. Note that this model using $x = 0.6$, which always assumes antiferromagnetic coupling of the interface and YIG, does not explain the total m well above ∼150 K.

We examine the issue of the T-driven change in interfacial alignment with a similar simple modeling approach in Fig. 7. Here we subtract the 15.9-nm-thick bulk YIG moment from the measured total moment of the film to give an estimated contribution of the interface moment, m_{int}. Figure 7 plots $-m_{int}$ determined from SQUID magnetometry (blue data points), along with the interfacial moment determined from PNR (red circles). These agree well for all T, and both show a crossover from AF to FM alignment (as indicated schematically) of the interfacial and YIG film moments. We again compare these moments with the published data for a range of $(Gd_xY_{1-x})_3Fe_5O_{12}$ layers, again assuming 3.6 nm thickness to calculate total moment. As seen in Fig. 6, the estimated interfacial component, especially at low T, matches best with mixed garnets with fairly large x. However the measured $-m_{int}$ is never large enough to match expectations for a simple pure GdIG layer. The most likely scenario is a distribution of Gd composition through the 3.6-nm film, with the average composition approximately between $x = 0.4$ and $x = 0.6$. We note that mixed garnets with this composition have ferrimagnetic compensation points, T_{comp}, near the T where the interfacial coupling of the interface and film reverse. The compensation point originates in the different T dependence of the moment of the Gd and Fe sublattices in the (Gd-Y)IG, such that T_{comp} indicates where the Fe sublattice has a larger contribution to the total moment than the Gd sublattice. The Fe sublattice could in turn show a tendency toward ferromagnetic exchange coupling to the entirely Fe sublattices of the YIG. We can adapt our very simple model to this situation by reversing the moment of the interfacial contribution above T_{comp}, which we show with the dotted blue and green lines for $x = 0.4$ and $x = 0.6$, respectively. The measured $-m_{int}$ from both SQUID and PNR falls between these lines.

If the crossover from AF to FM alignment of the interfacial layer and YIG in these heterostructures is indeed determined by the compensation point of the (Gd-Y)IG mixed garnet formed from interdiffusion at the interface, then one expects the T of the switch between AF and FM alignment of the two

films to be strongly dependent on the details of the interdiffusion and the average composition of the resulting mixed layer. In very high x interfacial layers, a reversal in coupling may not be observed until above 300 K, since T_{comp} for GIG falls near or above room T. It is also conceivable that heterogeneity of the composition of Gd in the interface layer could lead to a wide range of T_{comp} and competing interactions that could present as a nonmagnetic interfacial layer. This could explain the variation in previous reports of the magnetic character and alignment of the interfacial layer between GGG and YIG. Note that this simple analysis assumes that the magnetization of both the 15.9-nm-thick YIG and the 3.6-nm-thick (Gd-Y)IG films are essentially the same as bulk.

IV. CONCLUSIONS

In summary, we presented evidence for and characterization of a mixed Gd and Y garnet interface layer formed between an essentially bulk-like 15.9-nm-thick epitaxial YIG film and a GGG substrate. Using PNR and SQUID magnetometry, we show that antiferromagnetic alignment between the YIG and the interfacial layer of (Gd-Y)IG persists to very large fields at low temperature. In small (or zero) applied field both probes show a crossover from antiferromagnetic to ferromagnetic alignment of the interfacial and film moments. We suggest a possible correlation of this crossover with the ferrimagnetic compensation point in the (Gd-Y)IG mixed garnet that forms the interface, which in our case has a fairly high Gd content but is not entirely GIG. Variations in the interfacial layer composition will lead to variation in T_{comp}, which could explain discrepancies in earlier studies of the YIG/GGG system. The magnetic properties of this interface layer has potential impact on a wide range of studies involving YIG grown on GGG, from fundamental magnetism to magnonics and spintronics.

ACKNOWLEDGMENTS

We thank Y. Takamura, L. Hernandez, S. Bleser, R. K. Bennet, and M. Natale for helpful discussions and/or assistance in the laboratory. Work at DU was supported by the U.S. NSF (Grant No. DMR-1709646). Work at CSU was supported by the U.S. National Science Foundation (Grants No. EFMA-1641989; No. ECCS-1915849; No. DMR-2002980). Certain commercial products or company names are identified here to describe our study adequately. Such identification is not intended to imply recommendation or endorsement by the National Institute of Standards and Technology, nor is it intended to imply that the products or names identified are necessarily the best available for the purpose.

[1] A. A. Serga, A. V. Chumak, and B. Hillebrands, YIG magnonics, J. Phys. D **43**, 264002 (2010).

[2] A. V. Chumak, V. I. Vasyuchka, A. A. Serga, and B. Hillebrands, Magnon spintronics, Nat. Phys. **11**, 453 (2015).

[3] B. Heinrich, C. Burrowes, E. Montoya, B. Kardasz, E. Girt, Y.-Y. Song, Y. Sun, and M. Wu, Spin Pumping at the Magnetic Insulator (YIG)/Normal Metal (Au) Interfaces, Phys. Rev. Lett. **107**, 066604 (2011).

[4] M. Weiler, M. Althammer, F. D. Czeschka, H. Huebl, M. S. Wagner, M. Opel, I.-M. Imort, G. Reiss, A. Thomas, R. Gross, and S. T. B. Goennenwein, Local Charge and Spin Currents in Magnetothermal Landscapes, Phys. Rev. Lett. **108**, 106602 (2012).

[5] M. Weiler, M. Althammer, M. Schreier, J. Lotze, M. Pernpeintner, S. Meyer, H. Huebl, R. Gross, A. Kamra, J. Xiao, Y.-T. Chen, H. J. Jiao, G. E. W. Bauer, and S. T. B. Goennenwein, Experimental Test of the Spin Mixing Interface Conductivity Concept, Phys. Rev. Lett. **111**, 176601 (2013).

[6] H. L. Wang, C. H. Du, Y. Pu, R. Adur, P. C. Hammel, and F. Y. Yang, Large spin pumping from epitaxial $Y_3Fe_5O_{12}$ thin films to Pt and W layers, Phys. Rev. B **88**, 100406(R) (2013).

[7] M. Haertinger, C. H. Back, J. Lotze, M. Weiler, S. Geprägs, H. Huebl, S. T. B. Goennenwein, and G. Woltersdorf, Spin pumping in YIG/Pt bilayers as a function of layer thickness, Phys. Rev. B **92**, 054437 (2015).

[8] L. Liu, Y. Li, Y. Liu, T. Feng, J. Xu, X. R. Wang, D. Wu, P. Gao, and J. Li, Interfacial modulation of spin pumping in YIG/Pt, Phys. Rev. B **102**, 014411 (2020).

[9] K.-i. Uchida, H. Adachi, T. Ota, H. Nakayama, S. Maekawa, and E. Saitoh, Observation of longitudinal spin-Seebeck effect in magnetic insulators, Appl. Phys. Lett. **97**, 172505 (2010).

[10] K. Uchida, M. Ishida, T. Kikkawa, A. Kirihara, T. Murakami, and E. Saitoh, Longitudinal spin Seebeck effect: From fundamentals to applications, J. Phys.: Condens. Matter **26**, 343202 (2014).

[11] D. Qu, S. Y. Huang, J. Hu, R. Wu, and C. L. Chien, Intrinsic Spin Seebeck Effect in Au/YIG, Phys. Rev. Lett. **110**, 067206 (2013).

[12] D. Qu, S. Y. Huang, B. F. Miao, S. X. Huang, and C. L. Chien, Self-consistent determination of spin Hall angles in selected 5*d* metals by thermal spin injection, Phys. Rev. B **89**, 140407(R) (2014).

[13] L. J. Cornelissen, J. Liu, R. A. Duine, J. B. Youssef, and B. J. van Wees, Long-distance transport of magnon spin information in a magnetic insulator at room temperature, Nat. Phys. **11**, 1022 (2015).

[14] S. T. B. Goennenwein, R. Schlitz, M. Pernpeintner, K. Ganzhorn, M. Althammer, R. Gross, and H. Huebl, Non-local magnetoresistance in YIG/Pt nanostructures, Appl. Phys. Lett. **107**, 172405 (2015).

[15] L. J. Cornelissen and B. J. van Wees, Magnetic field dependence of the magnon spin diffusion length in the magnetic insulator yttrium iron garnet, Phys. Rev. B **93**, 020403(R) (2016).

[16] J. Shan, L. J. Cornelissen, N. Vlietstra, J. Ben Youssef, T. Kuschel, R. A. Duine, and B. J. van Wees, Influence of yttrium iron garnet thickness and heater opacity on the nonlocal transport of electrically and thermally excited magnons, Phys. Rev. B **94**, 174437 (2016).

[17] L. J. Cornelissen, J. Liu, B. J. van Wees, and R. A. Duine, Spin-Current-Controlled Modulation of the Magnon Spin Conductance in a Three-Terminal Magnon Transistor, Phys. Rev. Lett. **120**, 097702 (2018).

[18] H. Wu, L. Huang, C. Fang, B. S. Yang, C. H. Wan, G. Q. Yu, J. F. Feng, H. X. Wei, and X. F. Han, Magnon Valve Effect Between Two Magnetic Insulators, Phys. Rev. Lett. **120**, 097205 (2018).

[19] T. Wimmer, M. Althammer, L. Liensberger, N. Vlietstra, S. Geprägs, M. Weiler, R. Gross, and H. Huebl, Spin Transport in a Magnetic Insulator with Zero Effective Damping, Phys. Rev. Lett. **123**, 257201 (2019).

[20] G. Schmidt, C. Hauser, P. Trempler, M. Paleschke, and E. T. Papaioannou, Ultra thin films of yttrium iron garnet with very low damping: A review, Phys. Status Solidi B **257**, 1900644 (2020).

[21] Y. Fetisov, P. Kabos, and C. Patton, Active magnetostatic wave delay line, IEEE Trans. Magn. **34**, 259 (1998).

[22] A. D. Karenowska, A. V. Chumak, A. A. Serga, J. F. Gregg, and B. Hillebrands, Magnonic crystal based forced dominant wavenumber selection in a spin-wave active ring, Appl. Phys. Lett. **96**, 082505 (2010).

[23] E. Bankowski, T. Meitzler, R. S. Khymyn, V. S. Tiberkevich, A. N. Slavin, and H. X. Tang, Magnonic crystal as a delay line for low-noise auto-oscillators, Appl. Phys. Lett. **107**, 122409 (2015).

[24] A. D. Karenowska, J. F. Gregg, V. S. Tiberkevich, A. N. Slavin, A. V. Chumak, A. A. Serga, and B. Hillebrands, Oscillatory Energy Exchange Between Waves Coupled by a Dynamic Artificial Crystal, Phys. Rev. Lett. **108**, 015505 (2012).

[25] L. Sheng, J. Chen, H. Wang, and H. Yu, Magnonics based on thin-film iron garnets, J. Phys. Soc. Jpn. **90**, 081005 (2021).

[26] E. L. Jakubisova, S. Visnovsky, H. Chang, and M. Wu, Interface effects in nanometer-thick yttrium iron garnet films studied by magneto-optical spectroscopy, Appl. Phys. Lett. **108**, 082403 (2016).

[27] J. C. Gallagher, A. S. Yang, J. T. Brangham, B. D. Esser, S. P. White, M. R. Page, K.-Y. Meng, S. Yu, R. Adur, W. Ruane, S. R. Dunsiger, D. W. McComb, F. Yang, and P. C. Hammel, Exceptionally high magnetization of stoichiometric $Y_3Fe_5O_{12}$ epitaxial films grown on $Gd_3Ga_5O_{12}$, Appl. Phys. Lett. **109**, 072401 (2016).

[28] A. Mitra, O. Cespedes, Q. Ramasse, M. Ali, S. Marmion, M. Ward, R. M. D. Brydson, C. J. Kinane, J. F. K. Cooper, S. Langridge, and B. J. Hickey, Interfacial origin of the magnetisation suppression of thin film yttrium iron garnet, Sci. Rep. **7**, 11774 (2017).

[29] J. F. K. Cooper, C. J. Kinane, S. Langridge, M. Ali, B. J. Hickey, T. Niizeki, K. Uchida, E. Saitoh, H. Ambaye, and A. Glavic, Unexpected structural and magnetic depth dependence of YIG thin films, Phys. Rev. B **96**, 104404 (2017).

[30] J. M. Gomez-Perez, S. Vélez, L. McKenzie-Sell, M. Amado, J. Herrero-Martín, J. López-López, S. Blanco-Canosa, L. E. Hueso, A. Chuvilin, J. W. A. Robinson, and F. Casanova, Synthetic antiferromagnetic coupling between ultrathin insulating garnets, Phys. Rev. Appl. **10**, 044046 (2018).

[31] S. M. Suturin, A. M. Korovin, V. E. Bursian, L. V. Lutsev, V. Bourobina, N. L. Yakovlev, M. Montecchi, L. Pasquali, V. Ukleev, A. Vorobiev, A. Devishvili, and N. S. Sokolov, Role of gallium diffusion in the formation of a magnetically dead layer at the $Y_3Fe_5O_{12}/Gd_3Ga_5O_{12}$ epitaxial interface, Phys. Rev. Materials **2**, 104404 (2018).

[32] J. Fontcuberta, H. B. Vasili, J. Gàzquez, and F. Casanova, On the role of interfaces on spin transport in magnetic insulator/normal metal heterostructures, Adv. Mater. Interfaces **6**, 1900475 (2019).

[33] L. Wang, Z. Lu, X. Zhao, W. Zhang, Y. Chen, Y. Tian, S. Yan, L. Bai, and M. Harder, Magnetization coupling in a YIG/GGG structure, Phys. Rev. B **102**, 144428 (2020).

[34] R. Kumar, S. N. Sarangi, D. Samal, and Z. Hossain, Positive exchange bias and inverted hysteresis loop in $Y_3Fe_5O_{12}/Gd_3Ga_5O_{12}$, Phys. Rev. B **103**, 064421 (2021).

[35] F. Hellman, A. Hoffmann, Y. Tserkovnyak, G. S. D. Beach, E. E. Fullerton, C. Leighton, A. H. MacDonald, D. C. Ralph, D. A. Arena, H. A. Dürr, P. Fischer, J. Grollier, J. P. Heremans, T. Jungwirth, A. V. Kimel, B. Koopmans, I. N. Krivorotov, S. J. May, A. K. Petford-Long, J. M. Rondinelli *et al.*, Interface-induced phenomena in magnetism, Rev. Mod. Phys. **89**, 025006 (2017).

[36] R. C. LeCraw, E. M. Gyorgy, and R. Wolfe, Suppression of hard bubbles in LPE garnet films by inert atmosphere annealing, Appl. Phys. Lett. **24**, 573 (1974).

[37] T. Yamagishi, J. Awaka, Y. Kawashima, M. Uemura, S. Ebisu, S. Chikazawa, and S. Nagata, Ferrimagnetic order in the mixed garnet $(Y_{1-x}Gd_x)_3Fe_5O_{12}$, Philos. Mag. **85**, 1819 (2005).

[38] M. Haidar, M. Ranjbar, M. Balinsky, R. K. Dumas, S. Khartsev, and J. Åkerman, Thickness- and temperature-dependent magnetodynamic properties of yttrium iron garnet thin films, J. Appl. Phys. **117**, 17D119 (2015).

[39] P. Schiffer, A. P. Ramirez, D. A. Huse, P. L. Gammel, U. Yaron, D. J. Bishop, and A. J. Valentino, Frustration Induced Spin Freezing in a Site-Ordered Magnet: Gadolinium Gallium Garnet, Phys. Rev. Lett. **74**, 2379 (1995).

[40] H. Chang, P. Li, W. Zhang, T. Liu, A. Hoffmann, L. Deng, and M. Wu, Nanometer-thick yttrium iron garnet films with extremely low damping, IEEE Magn. Lett. **5**, 1 (2014).

[41] C. Hauser, T. Richter, N. Homonnay, C. Eisenschmidt, M. Qaid, H. Deniz, D. Hesse, M. Sawicki, S. G. Ebbinghaus, and G. Schmidt, Yttrium iron garnet thin films with very low damping obtained by recrystallization of amorphous material, Sci. Rep. **6**, 20827 (2016).

[42] J. Ding, T. Liu, H. Chang, and M. Wu, Sputtering growth of low-damping yttrium-iron-garnet thin films, IEEE Magn. Lett. **11**, 5502305 (2020).

[43] http://www.crystal-gmbh.com

[44] C. Majkrzak, K. O'Donovan, and N. Berk, Polarized neutron reflectometry, in *Neutron Scattering from Magnetic Materials* (Elsevier, Amsterdam, 2006), pp. 397–471.

[45] B. Maranville, W. R. II, and P. Kienzle, Reductus: A stateless python data reduction service with a browser front end, J. Appl. Crystallogr. **51**, 1500 (2018).

[46] B. Kirby, P. Kienzle, B. Maranville, N. Berk, J. Krycka, F. Heinrich, and C. Majkrzak, Phase-sensitive specular neutron reflectometry for imaging the nanometer scale composition depth profile of thin-film materials, Curr. Opin. Colloid Interface Sci. **17**, 44 (2012).

[47] H. Bai, X. Z. Zhan, G. Li, J. Su, Z. Z. Zhu, Y. Zhang, T. Zhu, and J. W. Cai, Characterization of YIG thin films and vacuum annealing effect by polarized neutron reflectometry and magnetotransport measurements, Appl. Phys. Lett. **115**, 182401 (2019).

[48] I. S. Anderson, P. J. Brown, J. M. Carpenter, G. Lander, R. Pynn, J. M. Rowe, O. Schärpf, V. F. Sears, and

B. T. M. Willis, Neutron techniques, in *International Tables for Crystallography* (International Union of Crystallography, Chester, England, 2006), pp. 430–487.

[49] J. Lynn and P. Seeger, Resonance effects in neutron scattering lengths of rare-earth nuclides, At. Data Nucl. Data Tables **44**, 191 (1990).

[50] B. B. Maranville, A. Green, and P. A. Kienzle, Distributed error-function roughness in refl1d reflectometry fitting program, arXiv:1801.04975.

[51] J. A. Vrugt, C. ter Braak, C. Diks, B. A. Robinson, J. M. Hyman, and D. Higdon, Accelerating Markov chain monte carlo simulation by differential evolution with self-adaptive randomized subspace sampling, Int. J. Nonlinear Sci. Numer. Simul. **10**, 273 (2009).

[52] http://www.qdusa.com.

[53] B. J. Kirby, L. Fallarino, P. Riego, B. B. Maranville, C. W. Miller, and A. Berger, Nanoscale magnetic localization in exchange strength modulated ferromagnets, Phys. Rev. B **98**, 064404 (2018).

[54] M. J. Roos and B. L. Zink, Apparent non-linear negative magnetization and exchange bias in paramagnetic substrates driven by trapped flux (unpublished).

[55] J. de la Venta, M. Erekhinsky, S. Wang, K. G. West, R. Morales, and I. K. Schuller, Exchange bias induced by the Fe_3O_4 Verwey transition, Phys. Rev. B **85**, 134447 (2012).

[56] S. J. Yuan, L. Li, T. F. Qi, L. E. DeLong, and G. Cao, Giant vertical magnetization shift induced by spin canting in a $Co/Ca_2Ru_{0.98}Fe_{0.02}FeO_4$ heterostructure, Phys. Rev. B **88**, 024413 (2013).

[57] R. Rana, P. Pandey, and D. S. Rana, Controlling the coexisting vertical magnetization shift and exchange bias in $La_{0.3}Sr_{0.7}FeO_3/SrRuO_3$ bilayers, Appl. Phys. Lett. **104**, 092413 (2014).

[58] M. J. Pechan, D. Bennett, N. Teng, C. Leighton, J. Nogués, and I. K. Schuller, Induced anisotropy and positive exchange bias: A temperature, angular, and cooling field study by ferromagnetic resonance, Phys. Rev. B **65**, 064410 (2002).

[59] C. Leighton, H. Suhl, M. J. Pechan, R. Compton, J. Nogués, and I. K. Schuller, Coercivity enhancement above the Néel temperature of an antiferromagnet/ferromagnet bilayer, J. Appl. Phys. **92**, 1483 (2002).

[60] M. Grimsditch, A. Hoffmann, P. Vavassori, H. Shi, and D. Lederman, Exchange-Induced Anisotropies at Ferromagnetic-Antiferromagnetic Interfaces Above and Below the Néel Temperature, Phys. Rev. Lett. **90**, 257201 (2003).

[61] E. Shipton, K. Chan, T. Hauet, O. Hellwig, and E. E. Fullerton, Suppression of the perpendicular anisotropy at the CoO Néel temperature in exchange-biased CoO/[Co/Pt] multilayers, Appl. Phys. Lett. **95**, 132509 (2009).

[62] B. L. Zink, M. Manno, L. O'Brien, J. Lotze, M. Weiler, D. Bassett, S. J. Mason, S. T. B. Goennenwein, M. Johnson, and C. Leighton, Efficient spin transport through native oxides of nickel and permalloy with platinum and gold overlayers, Phys. Rev. B **93**, 184401 (2016).